A stably stratified channel flow: Comparing a local similarity model with Direct Numerical Simulations

A.F. Moene*/B.J.H. van de Wiel+*
H.J.J. Jonker#

To be submitted J.A.S. Autumn 2010 in two (fully revised) parts

Abstract

In the present work a continuous turbulent stably stratified channel flow is studied with a direct numerical simulation model and with a simple similarity model. With DNS, the flow is simulated without the need of a specific turbulence closure model, whereas the local similarity model is based on a simple parameterization of turbulence. A relatively low Reynolds flow is simulated and both models explicitly account for molecular flux contributions. The flow configuration is identical to a study by Nieuwstadt. In spite of their different nature, both models give comparable results on the evolution of the mean and the flux profiles. Inspired by this the DNS results were used to calculate flux-profile relationships. The dimensionless gradients of wind and temperature from our DNS show strong evidence for log-linear behaviour close to the traditional $\phi_{M,H} = 1 + 5z/\Lambda$ over the range of analysis ($0 < z/\Lambda < 4$). This suggest that in an idealistic stationary and homogeneous flow, log-linear behaviour remains valid for strong stability. On the other hand, the current analysis is based on low Reynolds number flow and the sensitivity of the results on *Re* deserves more attention in future work.

(Keywords: Local similarity, Direct Numerical Simulation, Stable boundary layer, Collapse)

Affiliation authors + : Dept. Applied Physics, Eindhoven Technical University

Affiliation authors *: Dept. of Meteorology and Air Quality, Wageningen University and Research Centre.

Affiliation authors #: Dept. of Multi-Scale Physics, Delft University of Technology,

Corresponding author:

B. J. H. van de Wiel,
Turbulence and Vortex Dynamics
Department of Applied Physics,
Eindhoven
Technical University, The Netherlands.
E-mail: b.j.h.v.d.wiel@tue.nl

1 Introduction

For many purposes related to meteorology and climate a proper understanding of the boundary layer processes in stably stratified conditions is essential (Beljaars and Viterbo, 1998). In spite of its importance, a true general framework of the stable boundary layer (SBL) is still lacking. In absence of a framework, it appears useful to classify stable boundary layers into two major prototypes (Mahrt et al., 1998):

- *The Weakly Stable Boundary Layer (WSBL)*
- *The Very Stable Boundary Layer (VSBL)*

Weakly stable boundary layers are characterized by the presence of continuous turbulence and tend to occur in windy and/or cloudy conditions. This type of boundary layer is generally rather well-understood and both fluxes and profiles more or less obey the local similarity scaling as formulated by Nieuwstadt (1984). Therefore, for most practical modeling applications our representations of the WSBL are acceptable to some degree (Galmarini et al., 1998; Basu et al, 2006; Sorbjan, 2006; Steeneveld et al., 2006).

In contrast the *very stable boundary layer* is poorly understood. This type of boundary layer is characterized by the occurrence of turbulence that is discontinuous in time (intermittent) and usually rather weak or virtually absent. In the latter case we may speak of a so-called radiative SBL, due to the fact that, in the absence of turbulent heat transport, radiation and soil heat conduction are the dominant thermodynamic processes (Van de Wiel et al. 2003). Even though a complete picture of the VSBL does not exist, considerable effort has been made in recent years to characterize important features of the SBL under strongly stratified conditions. Especially, extensive field campaigns such as CASES99 (Poulos, 2002) facilitated detailed characterization of e.g.: drainage flow, (Mahrt et al., 2001), low-level jet formation (Banta, 2007), intermittent turbulent events and flow instabilities (Sun et al., 2003; Newsome and Banta, 2002, Van de Wiel et al., 2003), longwave radiative divergence (Sun et al., 2003) and soil heat transport (Van de Wiel et al., 2003 -App. A).
Although the aforementioned classification into WSBL and VSBL is a useful concept, a formal physical criterion for existence of different SBL regimes does not exist. It is not clear why and when turbulence in the WSBL 'gives up' and loses its continuous character, and it seems that the transition of the WSLB to the VSBL is one of the key-standing challenges in boundary layer meteorology (Nappo and Johanssson, 1999; Derbyshire, 1999a).

A new perspective to this problem was given by McNider et al. (1995). By analyzing a truncated model of the SBL they showed that regime transitions (from WSBL to VSBL), are a natural consequence of the non-linearity in the diffusion terms of the governing equations. Intuitively, this nonlinear response can be appreciated from basic gradient thinking (Malhi, 1995, Van de Wiel et al. 2007, Basu et al. 2007):

- In case of weak stratification a sudden increase in the vertical temperature gradient generally causes a larger downward heat flux, which opposes the disturbance (negative feedback). Turbulence is able to maintain its continuous character.
- In case of strong stratification, a sudden increase in the vertical temperature gradient causes a significant decrease of the turbulent diffusivity, which may lead to a smaller flux so that the disturbance is enhanced (positive feedback). In this case turbulence tends to collapse.

In Derbyshire (1999b from now on: D99b) an analysis similar to McNider et al. (1995) is performed, but with a more realistic type of model, resembling typical weather forecast models with respect to its stable boundary layer parameterizations. Intriguing results are shown in a sense that model instability depends on both the turbulent parameterizations and on land surface characteristics. Moreover, from theoretical analysis on linear wind and temperature profiles, D99b suggested that this instability is a true physical, hydrodynamic instability. An innovative aspect in the analysis is that he performed linear stability analyses (LSA) on heavily *parameterized equations.* To appreciate this, it is important to realize that in a classical sense, LSA is applied to *exact* solutions of the equations of motion (Nieuwstadt, 1992). For example: linear perturbations of the inviscid Boussinesq equations in stably stratified flow are governed by the well-known Taylor-Goldstein equation. From this, Miles (1961) and Howard (1961) showed that a necessary condition for instability of a linearly stratified flow is $Ri < 1/4$. This criterion is generally used as a predictor for the transition from stably stratified laminar to turbulent flow.
It is tempting to apply the theory of hydrodynamic stability also to the reverse problem: predicting collapse of a turbulent stratified flow towards a laminar state (~from WSBL to VSBL). However, this is not straightforward, as closed-form analytical solutions of the turbulent reference state, needed to impose perturbations on, are generally unavailable.

The problem is circumvented by analyzing a parameterized set of equations for the turbulence. Of course the success of the method mainly depends on the validity of the parameterization itself. Unfortunately, the linear profiles in D99b are rather unrealistic for the atmospheric SBL, where profiles become logarithmic close to the surface. Therefore, Van de Wiel et al. (2007) extended the work of D99b to realistic profiles. They analyzed the hydrodynamic stability of log-linear profiles in a plate-driven Couette flow and were able to predict the collapse of turbulence in terms of the external forcing parameters.

Despite those promising results, the studies heavily depend on the adopted closure assumptions. Also, in order to make the mathematical analysis tractable, forcings and boundary conditions are rather unrealistic as compared to the atmosphere. In fact, true progress can only be made by comparing the analysis with observed regime transitions. It is clear that such a comparison is not a trivial task, as the real atmosphere has ‘open borders’, is non-homogeneous and often non-stationary (e.g. Vickers et al., 2006).
Alternatively, we may compare the analysis with direct numerical simulations (DNS) of the SBL. In a DNS the Navier-Stokes equations are discretized directly without the need of a specific turbulence closure assumption, which is an advantage over e.g. Large Eddy Simulation (Nieuwstadt, 1992). Also, it is possible to control the flow in terms of forcing parameters and pure stationary homogeneous situations can be studied. Nevertheless, it is realized that a DNS of a stably stratified flow is still only a surrogate of the real SBL: due to limited computational power, DNS-studies typically simulate flows with Reynolds numbers of $O(10^4\text{-}10^5)$ as typical atmospheric value are $O(10^8\text{-}10^9)$. Moreover, important processes like longwave radiative divergence are usually neglected in DNS and the surface is often taken as an external boundary condition, although in reality it is an internal part of the system leading to additional feedbacks (Van de Wiel et al. 2002a).

In this context, an important result was obtained recently, by Nieuwstadt (2005), from now on N05. N05 used a DNS to study a pressure-driven stably stratified channel flow with a fixed surface heat flux. By altering the surface heat flux, a regime transition from a continuous SBL to a non-turbulent SBL was observed, similar to the atmospheric case. This is illustrated in figure 1, where we repeated the N05 simulations: two cooling rates reflecting two different values of the stability parameter h/L, are imposed. The figure shows the turbulent kinetic energy (TKE) as a function of time. For h/L=0.4 the TKE approaches a steady state: a continuous turbulent SBL. For h/L=2.0, however, the TKE rapidly decreases because of ceasing turbulence. Apparently, the system's response is highly non-linear (not 'smooth') for increased cooling.

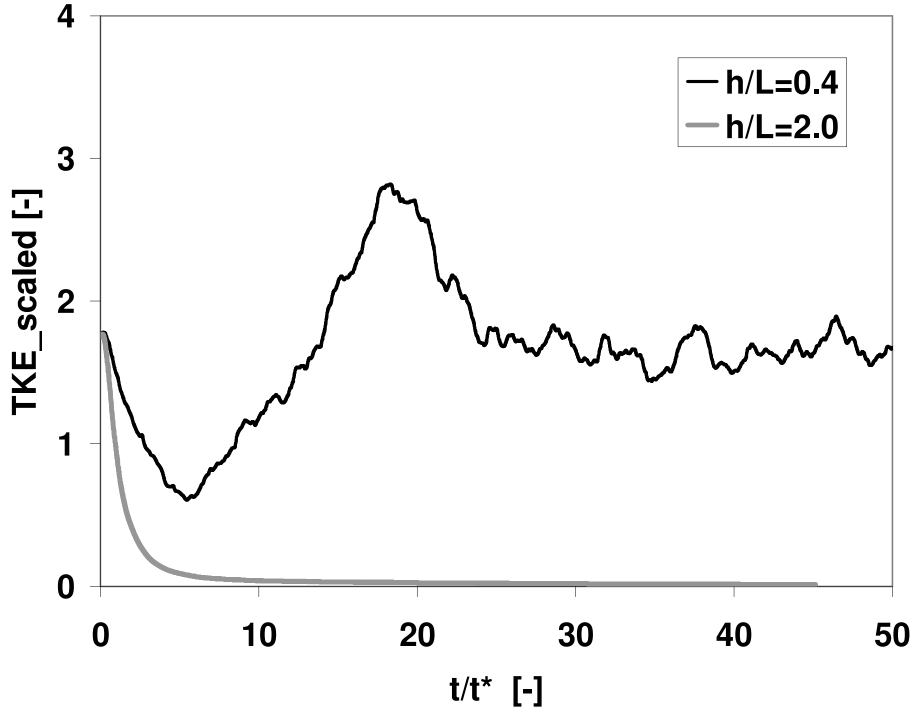

Fig. 1. Time evolution of the turbulent kinetic energy (scaled by pressure gradient and channel depth-section 2) in a stably stratified channel flow. The cases represent moderate cooling (black line) and strong cooling (grev line). Results are obtained from DNS as described in section 2.

Moreover, circumstantial evidence was given in N05 suggesting that the DNS profiles may still follow local similarity scaling, in spite of the low Reynolds numbers (see also: Coleman et al. 1992). This aspect is of significance and will be elaborated in the present study, because local similarity is the cornerstone for the parametization of turbulence in the abovementioned theoretical models. As such we focus on the continuous turbulent stratified flow depicted in figure 1 (case 1). Direct numerical simulations will be compared with results from a local-similarity model. As such, we explore the N05 conjecture and will show that local similarity is still valid at those low Reynolds numbers. This conclusion enables us to use DNS as a tool to diagnose the shape of the local similarity functions for the gradients of wind and temperature, without the need to rely on a closure assumption. It provides 'benchmark similarity-relationships' for idealistic stationary homogeneous flow, complementary to atmospheric similarity studies that are often disturbed by non-stationary and non-homogeneous effects (Mahrt, 2007). In future work the collapse case will be studied in more detail (second case in Fig. 1), as to investigate a possible analogy between DNS and similarity models for this case and to investigate the potential of the theoretical approach mentioned above (D99b, W07).

The paper is organized as follows: in section 2 the simulation set-up and the model descriptions are given. The results of the model comparison are shown for the neutral spin-up and the cooling period in section 3 and 4, respectively. In section 5 similarity functions for the dimensionless gradient are determined from DNS simulations, followed by discussion and conclusions in sections 6 and 7.

2 Set-up of the numerical experiment and model descriptions

As an analogy to atmospheric stratified flows, N05 studied a simple stably stratified channel flow. We adopt the same configuration using:

- A direct numerical simulation model (DNS), that resolves turbulence up to the Kolmogorov scale.
- A local similarity based model

2.1 Set up of the experiment and flow configuration

Aerodynamic smooth flow is simulated with a turbulent Reynolds number $\mathrm{Re}_* = u_{*EXT}\, h/\nu = 360$, where the value of u_{*EXT} equals the surface friction velocity, u_{*0}, in steady state (see below), h is the channel depth and ν the kinematic viscosity of the fluid. In terms of mean bulk velocity, assuming $U_{bulk}/u_* \approx O(20)$, the bulk Reynolds number is $O(7000)$. Obviously, the Reynolds number is small as compared to typical atmospheric values (say ~ $O(10^8)$), due to computational limitations of DNS. This aspect will be discussed in section 4.

A schematic picture of the configuration is given in figure 2.

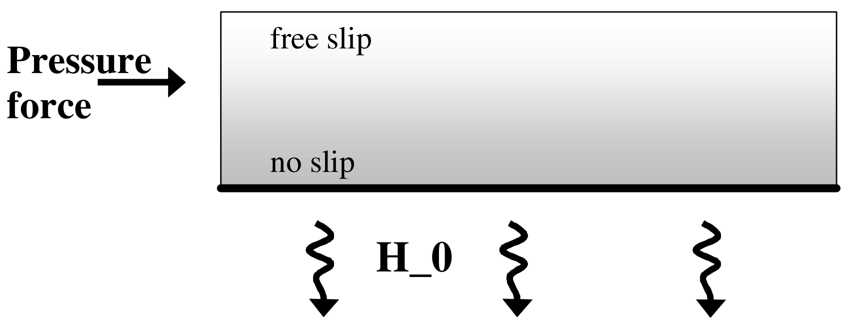

Fig. 2: schematic picture of the channel flow. Decreasing temperature is reflected by increasing grey-scale.

Mechanical forcing:

-A horizontal pressure gradient is imposed such that: $\mathrm{Re}_* = u_{*EXT} h/\nu = 360$ with $u_{*EXT} = \sqrt{-(1/\rho)(\partial P/\partial x)h}$, and fixed channel height h. The external forcing parameter u_{*EXT} equals surface friction velocity u_{*0} in a steady state (Eq. (6)).

Boundary conditions:

-At the lower boundary the amount of heat extracted at the surface H_0 is prescribed (Von Neumann condition) by fixing the external parameter h/L_{EXT} to the default value 0.4. h/L_{EXT} is defined by:

$$h/L_{EXT} = \frac{\kappa g h}{T_{ref}\,\rho c_p} \cdot \frac{H_0}{u_{*EXT}^3} \tag{1}$$

It is important to note that, contrary to N05, we include the Von Karman constant in the definition of L, following meteorological conventions. Thus, our $h/L_{EXT} = 0.4$ must be

compared with the N05 $h/L_{EXT} = 1.0$ case. In summary: the external 'drivers' of the system, the pressure gradient and the surface heat flux are *imposed* by fixing Re_* and h/L_{EXT} .
-The temperature at the top of the channel is fixed (Dirichlet condition).
-A no slip boundary is imposed at the bottom ($U = 0$ at $z = 0$), and a free-slip condition is imposed at the top ($\partial U/\partial z = 0$ at $z = h$).

Physical parameters:
For consistency with N05, the Prandtl number $\mathrm{Pr} = \nu/\lambda$ is set to unity, although 0.72 seems more realistic for atmospheric dry air. Coriolis effects are ignored and long-wave radiative divergence is not taken into account. The Von Kármán constant κ is set to 0.4 (Högström, 1996).

2.2 Direct numerical simulation (DNS)

In addition to the setup outlined above, for the DNS the following characteristics are relevant:

- The domain size is $5h$ in both horizontal directions and $1h$ in the wall-normal direction.
- The number of grid points is 100 in each of the three dimensions (unless stated otherwise).
- Periodic boundary conditions are applied to all variables in both horizontal directions.
- The initial conditions for the neutral runs ($h/L_{EXT} = 0$) are uniform temperature and uniform velocity (with some random perturbation). For the stratified runs, the initial conditions are obtained from that neutral run (run until equilibrium is reached).

The model was specifically developed for the present study although implementation details are similar to those in the LES model of Moene (2003). Note that we utilize a second-order finite volume discretization in space and for time integration a second-order Adams-Bashforth method is used.

Given the configuration, it is useful to establish whether a 100^3 grid suffices for DNS of a $\mathrm{Re}_* = 360$ flow, summarizing the analysis by N05. Consider an equilibrium flow situation and assume that the height averaged dissipation $\langle \varepsilon \rangle$ of TKE equals the average shear production:

$$\langle \varepsilon \rangle \approx \frac{1}{h}\int_0^h u_*^2(z)\frac{\partial U}{\partial z}dz = \frac{1}{h}\left[U\,u_*^2\right]_0^h - \frac{1}{h}\int_0^h U\frac{\partial u_*^2}{\partial z}dz \tag{2}$$

$u_*^2(z)$ is used as a short-hand notation for the local shear stress (the surface value of u_* is denoted by u_{*0}). The first term at the right hand side drops out and we realize that in an equilibrium state stress divergence is height-independent: $\partial u_*^2/\partial z = (1/\rho)(\partial P/\partial x)$, so that we obtain an estimate for the average dissipation:

$$\langle \varepsilon \rangle \approx -\frac{1}{\rho}\frac{\partial P}{\partial x}\langle U \rangle \tag{3}$$

with $\langle U \rangle$, the height-averaged velocity. From this dissipation rate the Kolmogorov length scale η is found:

$$\eta = \left(\frac{\langle \varepsilon \rangle}{\nu^3} \right)^{-\frac{1}{4}} \tag{4}$$

It should be stressed that this estimate of η is based on the domain averaged dissipation rate. Close to the surface both shear stress and shear will be relatively large and hence the production and dissipation of TKE, resulting in a smaller η. We combine (3) and (4) with the definition of Re_* to obtain the ratio between the domain height and the Kolmogorov length:

$$\frac{h}{\eta} = \left(\frac{\langle U \rangle}{u_{*EXT}} \mathrm{Re}_*^3 \right)^{\frac{1}{4}} \tag{5}$$

With $\mathrm{Re}_* = 360$ and a typical value for $\langle U \rangle / u_{*EXT} \cong 20$, we estimate: $h/\eta \cong 175$. From the number of grid cells $h/\Delta z = 100$, so that $\Delta z/\eta \cong 1.75$ and $\Delta x/\eta = \Delta y/\eta \cong 9$. As discussed in N05 this is at the limit of what one could call a DNS, and we accept it for our problem because the effects of static stability manifest themselves at scales much larger that η. Nevertheless, in section 5, we will discuss the grid resolution aspect by showing higher resolution results. For consistency with N05 we take a 100^3 grid as the default configuration.

2.3 A simple 1-D similarity model of stratified flow

For the similarity model the governing equations for wind speed and temperature read:

$$\frac{\partial U}{\partial t} = -\frac{1}{\rho}\frac{\partial P}{\partial x} + \frac{1}{\rho}\frac{\partial \tau}{\partial z} \tag{6}$$

$$\frac{\partial T}{\partial t} = -\frac{1}{\rho c_p}\frac{\partial H}{\partial z} \tag{7}$$

First order closure (K-theory) is adopted to parameterize the local stress τ and heat flux H:

$$\frac{\tau}{\rho} = K_{TOT,M} \frac{\partial U}{\partial z} \tag{8}$$

$$\frac{H}{\rho c_p} = -K_{TOT,H} \frac{\partial T}{\partial z} \tag{9}$$

The total diffusivities are taken to be the sum of molecular and turbulent contributions:

$$K_{TOT,M} = \nu + K_M \quad ; K_{TOT,H} = \lambda + K_H$$

(10)

From a physical point of view the turbulent diffusivities should take into account the limiting effects on dominant eddy size of both stability and the presence of a solid boundary (Van de Wiel *et al.* 2008). As such, the turbulent diffusivities are given by:

$$K_{M,H} = l_n^2 \left|\partial U/\partial z\right| f(Ri)$$

(11)

with l_n being the neutral mixing length and:

$$f(Ri) = (1 - Ri/R_c)^2; \qquad Ri \le R_c$$
$$f(Ri) = 0; \qquad Ri > R_c$$

(12)

Here, the gradient Richardson number is defined as:

$$Ri \equiv \frac{g}{T_{ref}} \frac{\partial T/\partial z}{(\partial U/\partial z)^2}$$

Van de Wiel et al. (2008) point out that (12) is equivalent to log-linear similarity functions:

$$\phi_{M,H} = 1 + \alpha \frac{z}{\Lambda}$$

(13)

Where ϕ_M and ϕ_H are the dimensionless wind speed and temperature gradients, respectively and Λ the local Obukhov length (Eq. (19)). Equivalence with (12) occurs when R_c is taken equal to $1/\alpha$ and $l_n = \kappa z$. We take $\alpha = 5$ ($R_c = 0.2$), as a reasonable representation (up to $z/\Lambda \sim O(1)$) of atmospheric observational studies (Businger et al. 1971, Högström (1996), Howell and Sun (1999), Baas et al. (2006)). The neutral mixing length l_n is given by:

$$l_n = A(z)\kappa z$$

(14)

At first sight this formulation seems to deviate from the classical $l_n = \kappa z$. However $A(z)$ virtually equals 1, except very close to the wall, for reasons given below (Pope, 2000; Kundu, 1990). In smooth flow the near-wall region can be divided into three sub-regions:

- *The viscous sublayer* with extends approximately from $0 < y^+ \le 5$, with $y^+ = u_* z/\upsilon$. The velocity profile is linear, being dominated by viscosity.
- *The inertial sublayer* that becomes valid for $y^+ > 30$. In this region "inertial" transfer of energy by inviscid turbulent motions dominates. The velocity profile attains the well-known logarithmic shape.

- *The buffer layer (* $5 < y^{+} \le 30$ *).* In this transitional layer neither viscous stress nor Reynolds stresses are negligible.

Although the asymptotic velocity profiles in the viscous sublayer and the inertial sublayer are readily found from (10)-(11) in combination with $l_n = \kappa z$ alone, it does not provide an accurate description of the profile in the buffer-layer. Based on laboratory studiesVan Driest (1956) found an empirical answer to this problem by defining a *damping function* $A(z)$ to be combined with (14):

$$A(z)=\left(1-\exp(-\frac{1}{C}\frac{u_* z}{\nu})\right) \quad \textbf{(15)}$$

,with the empirical constant $C \approx 26$. Note that expression (15) provides the correct physical limits in the viscous and the inertial sub-layer. It will be shown that Eqs. (10)-(15) give a reasonable representation of the velocity profile as compared to DNS.

2.4 A comment on the implementation of the upper boundary condition

Although the model comparison between the similarity model and the DNS is as 'clean as possible' the free-slip top boundary condition invokes an implementation issue that is inherent to the different nature of the models. By definition the vertical velocity vanishes at the top of the domain. For the DNS, this necessarily implies that velocity fluctuations at the top become zero ($w'=0$) and that turbulent exchange near the upper boundary is effectively suppressed. However, this 'upper-wall' damping effect is absent in simulations with the similarity model (where only mean velocities are dealt with and the mean vertical velocity is zero throughout the 1-D model). Fortunately, for the stably stratified case, turbulence in both models is strongly suppressed by the physical fact that $Ri \to R_c$ in the upper part of the domain (section 4). Therefore, consequences of this boundary issue mostly affect the neutral spin-up simulation, and effects on our case of interest (stratified flow) are limited. We note that the upper boundary issue could be avoided by simulating a vertically symmetric stably stratified Couette flow with two walls moving in opposite direction (with fixed wall temperatures). Such flow rapidly evolves towards a steady state as compared to the present pressure driven flow. Though it was verified that a close agreement between the similarity model and the DNS was reached, the results are beyond the scope of the present work.

3 Model comparison: neutral spin-up results

3.1 Introduction

In the next two sections we compare the results of a channel flow simulation with the 1-D similarity model (from now: 1-D) and the DNS. Both models start with an initial uniform wind profile: $U/u_*(z) = 30$. To ensure stationarity a relatively long neutral spin-up period of $50t_*$ is taken. We note that $50t_*$ is comparable to a time span of about 7 hours for an atmospheric SBL with $h = 100$ [m] and $u_* = 0.2$ [m s^{-1}] ($t_* = 500$ [s]). It was verified that a steady state was reached by analyzing both domain integrated TKE and mean profiles.

3.2 Results

In figure 3 we show the equilibrium velocity profiles as obtained by the numerical models. Although in general the results from the both models are rather close, some differences can be discerned. At the top of the channel the 1-D model seems to underestimate the velocity compared to the DNS (discussed below). In the lowest part of the channel both models seem to compare well, although this becomes more evident by plotting the flow in a classical sense, using a scaled height coordinate $z u_* / \nu$ on a horizontal logarithmic axis (Fig. 3b), where the scale parameter ν / u_* is proportional to the thickness of the viscous sub-layer.

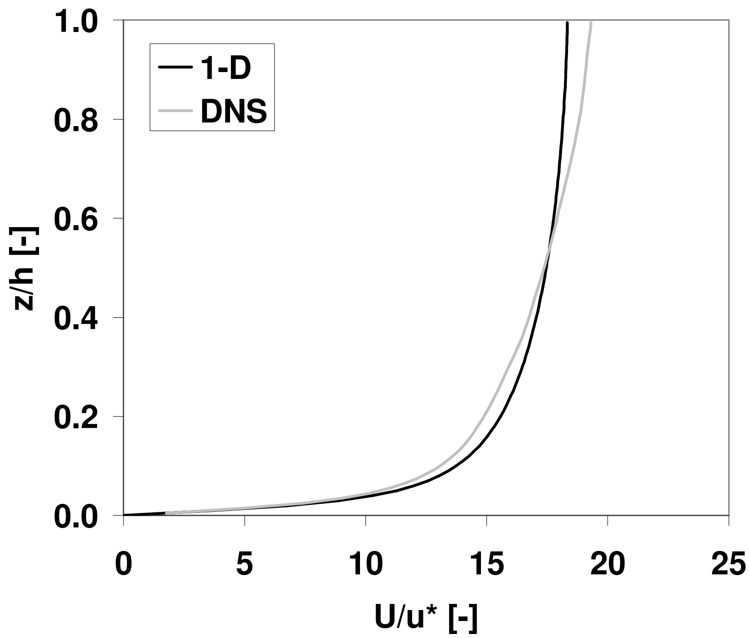

Fig. 3a: Equilibrium wind profiles after the neutral spin-up period.

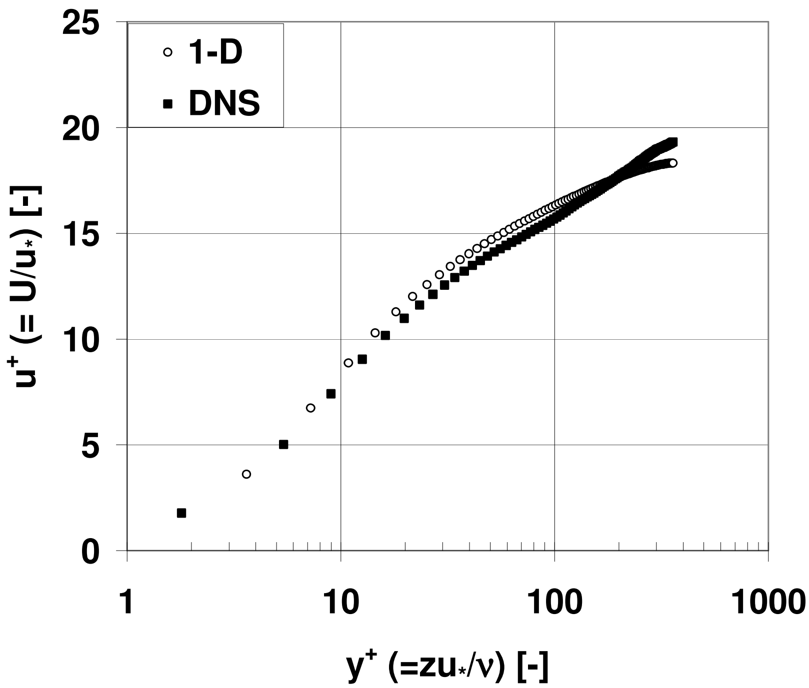

Fig. 3b: As 3a but now on a logarithmic scale using y+ height coordinates.

For y+>30 both models show a more or less logarithmic behaviour of the velocity profile (the well-known 'log-law of the wall'; not shown). Also, due to the fact that the 1-D model has proper physical limits in the viscous sublayer (u+=y+) and realistic velocity profile in the buffer layer (via the Van Driest function) the model is in good agreement with the DNS close to the wall.
Although Figs. 3a and 3b represent neutral flow, a the behavior close to the wall will be similar in the stably stratified case (next section). This can be understood by supposing that stability is of minor importance when say $z < 0.1L$ (Eq. (13)). For our default case with $h/L = 0.4$ this implies minor importance in the region $z < 0.25h$ or in viscous units: $y^+ < 0.25\,\mathrm{Re}_* = 90$. As such, close to the wall, good agreement between the 1-D and the DNS is to be expected for the stably stratified simulations as well.

Finally, as indicated above, it occurs that the 1-D model deviates from the DNS near the channel top. This is probably caused by the difference in the implementation of the top-boundary condition, discussed in section 2: as the DNS follows the $w' = 0$ condition at the top of our 'free-slip wall', there is a damping mechanism on turbulent exchange, which is absent in the 1-D case. Therefore, in order to oppose the same pressure gradient as in the 1-D case, the overall shear in the DNS must be larger.

4 Model comparison: results on stably stratified flow

4.1 1-D versus DNS: mean profiles

In this section the model comparison is extended to stably stratified flow, with the flow set-up consistent with Nieuwstadt (2005). After the neutral spin-up period, a fixed surface heat flux H_0 is extracted such that $h/L_{EXT} = 0.4$. As, contrary to N05, our definition of L includes the Von Karman constant, our $h/L_{EXT} = 0.4$ must be compared with the N05 $h/L_{EXT} = 1.0$ case. The integration period amounts $25t_*$, as in N05. For the DNS, mean variables are calculated from instantaneous horizontal slab-averages of the turbulent field.

Figure 4a shows the time evolution of the mean wind profile for the DNS. The effect of static stability is clearly visible. Due to the fact that turbulent exchange is less efficient in stratified flow as compared to neutral conditions, larger wind shear is needed to oppose the horizontal pressure gradient. The profile attains a typical log-linear shape that is also characteristic for atmospheric stably stratified conditions. At the channel top the wind speed gradient necessarily becomes zero due to the free-slip condition. Fig. 4b is similar to 4a, but now for the 1-D model. Although minor differences are noticeable, the agreement between the models is surprisingly good, in view of the fact that the 1-D model has relatively simple physics. The 1-D model gives the same characteristic wind profile: linear in the viscous sublayer, then log-shaped (inertial sublayer), again linear (dominated by static stability) and negatively curved at the top (due to the BC). Both models seem to reach a reasonable quasi-steady state after $25t_*$ although a strict steady state has not yet developed (see below).

A similar comparison is made for temperature (Figs. 5a,b). After a transient period, the temperature profiles approach some kind of quasi-steady equilibrium. By quasi-steady we mean that the *shape* of the temperature profile does not change in time. Of course, due to the fact that the boundary layer is cooling as a whole, the absolute temperature decreases. Formally, we speak of a quasi-steady equilibrium when (differentiating (7) with respect to z):

$$\frac{\partial}{\partial z}\frac{\partial T}{\partial t} = \frac{\partial}{\partial t}\left(\frac{\partial T}{\partial z}\right) = 0 = -\frac{1}{\rho c_p}\frac{\partial^2 H}{\partial z^2} \quad \textbf{(16)}$$

, which implies a linear flux profile. Due to the fact that a fixed temperature is prescribed at the top, a *truly* quasi steady state as in (16) can not be reached: as the boundary layer continues to cool as a whole, the temperature gradient at the top increases in time, so that (16) can not be valid at the top itself. In turn, the increasing gradient results in an increasing top heat flux by molecular diffusion. This non-negligible (relatively low Re) source of heat already reaches 40% of the surface heat flux at $25t_*$ and attains asymptotically 100% at t_* ~O(500). In the latter case, a constant flux layer is formed which implies strict stationarity ($\partial U/\partial t = \partial T/\partial t = 0$).

As for wind speed, the similarity between the simulated temperature profiles (5a,b) is strong except for some deviations during the transient period ($t = 10t_*$) where the integrated cooling in the 1-D model seems to be a bit less than in the DNS. It appears that a larger heat flux at the top of the boundary layer is generated in the 1-D case as compared to the DNS: at $t = 10t_*$ the1-D top heat flux is 12% of H_0 against 6.5% for the DNS. Although top temperatures are fixed, top-gradients and top molecular fluxes are not, being determined by the internal mixing characteristics of the system. Note that the previous discussion on the difference between the models in term of their top boundary condition may apply here as well, albeit of less importance than in the neutral case.

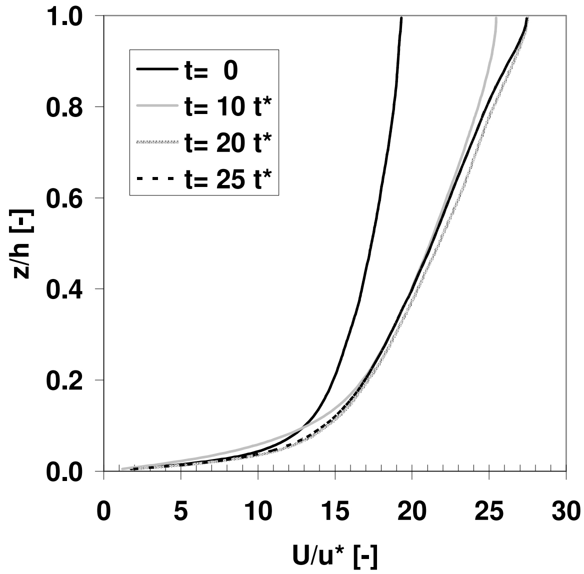

Fig. 4a: Temporal evolution of the wind profile as calculated by the Direct Numerical Simulation.

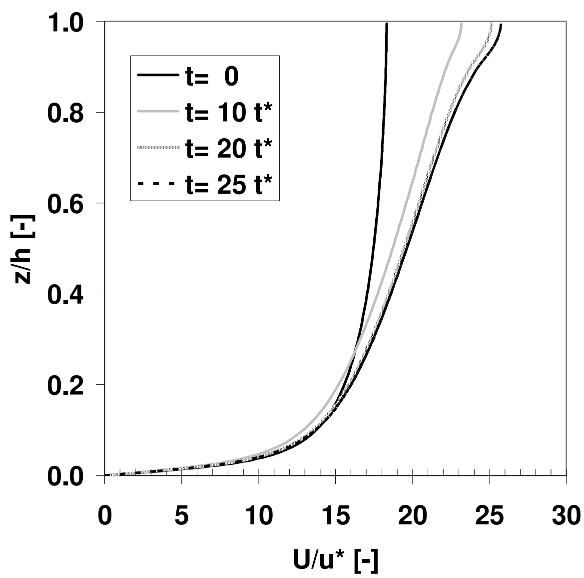

Fig. 4b: As 4a but now for the 1-D model

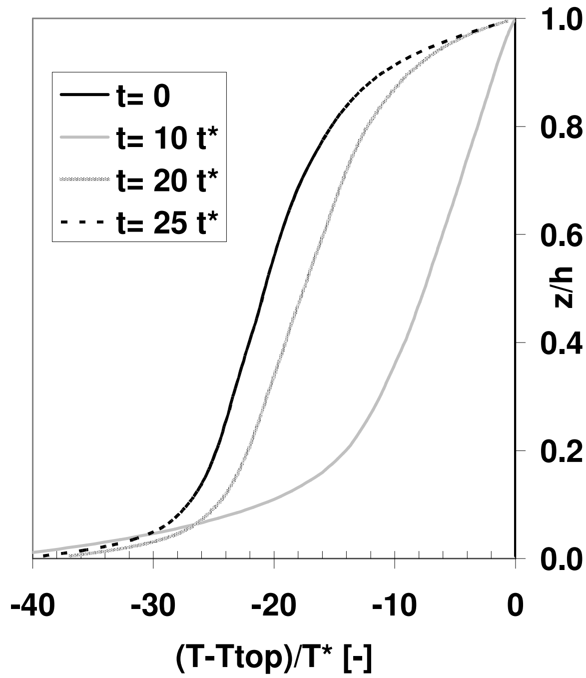

Fig. 5a: Temporal evolution of the temperature profile as calculated by the Direct Numerical Simulation.

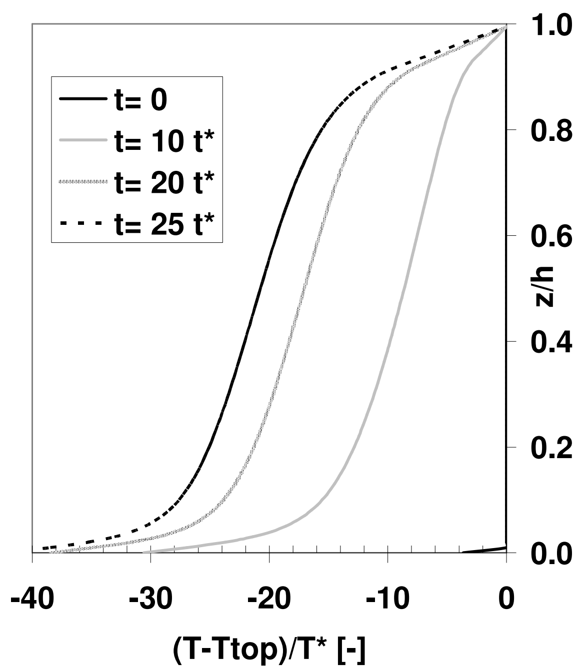

Fig. 5b: As 5a but now for the 1-D model

4.2 The DNS related to Nieuwstadt (2005): a short comment

Before proceeding to the flux profiles, the mean profiles of our DNS are compared with those from the DNS by Nieuwstadt (2005). This DNS-intercomparison is to support the idea that direct simulation does not require (subgrid) models of turbulence: 'different' DNS models should lead to equal results in an 'ensemble sense'. We obtained the N05 graphs by a data digitalization method, which is reasonably accurate except very close to the surface. Mean profiles after $t = 25t_*$ are shown in Figs. 6a,b.

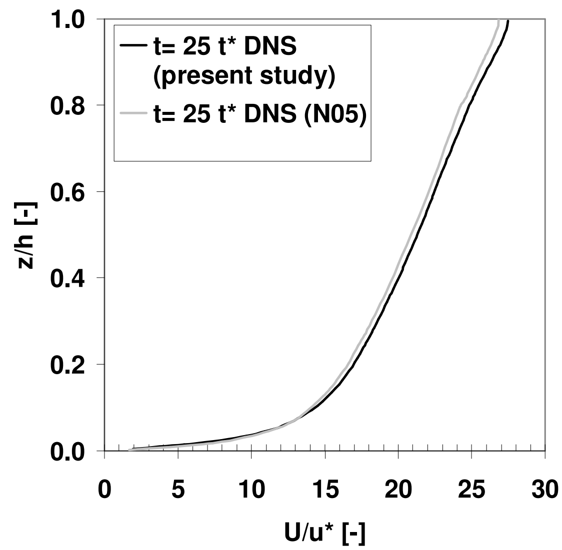

Fig. 6a: mean wind profile at t=25 t* for our and Nieuwstadt's DNS.

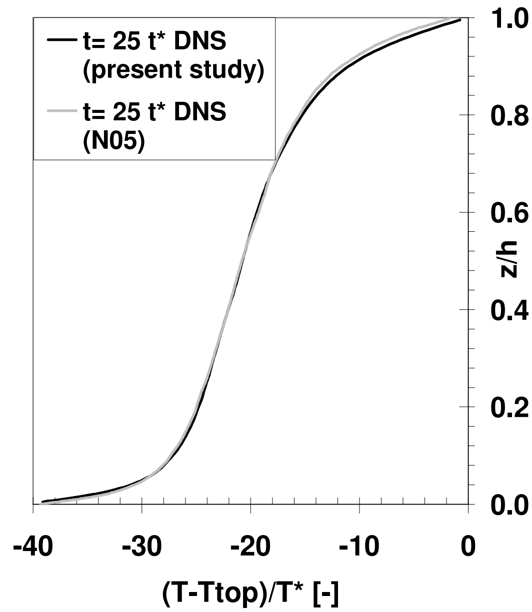

Fig. 6b: mean temperature profile at t=25 t*.

Although the models were developed independently, it is clear that both for wind and temperature an excellent agreement is found. Minor differences are supposed to be caused by either real statistical-physical effects: the mean profiles are (horizontally averaged) snapshots of *fluctuating* turbulent fields (formally speaking, confidence intervals should be used), by minor differences in the numerical techniques used to solve the equations, or different spin-up periods (not reported in N05). Figs. 6a, b may also be viewed upon as an independent confirmation of the N05 results. Keeping this in mind, we will focus on the comparison between our DNS and the 1-D model. A full DNS inter-comparison of turbulent fields is beyond the scope of this text.

4.3 1-D versus DNS: flux profiles

In Fig. 7a the DNS slab-averaged, instantaneous ($t = 25t_*$) flux-profiles are presented. The turbulent momentum flux has reached a nearly linear shape that is typical for this type of wall-shear flows that approach quasi-steady equilibrium. In fact, the linear shape is even more evident from the total momentum flux (turbulent + viscous transport, not shown): near the wall, turbulent motions are suppressed and shear is large, so that the momentum flux is dominated by viscous transport in that region. A characteristic linear profile is also observed for turbulent heat flux. However, the total heat flux (not shown) does not approach zero at the top. In fact, as the laminar heat flux at the top approaches 50% of the surface heat flux, so does the total heat flux. Similar characteristics are found for the 1-D model (Fig. 7b). As such, it appears that the simple superposition principle in the 1-D model with separate molecular and turbulent contributions to the total diffusion works reasonably well. Of course, due to the fact that the DNS model explicitly calculates turbulent motions, its patterns are more irregular than with our 1-D model that represents an ‘ensemble’.

Finally, the 1-D results are different for $z/h > 0.9$, because turbulent fluxes are diagnosed as zero, whenever $Ri > R_c$, according to Eq. (12). The time evolution of Ri in the 1-D model is given in Fig. 8, together with a single Ri-profile from the DNS. Generally, the Ri-profiles develop a typical negative curvature. For all times indicated, Ri exceeds R_c at the top of the channel. For $t \geq 10t_*$, $Ri >= \frac{1}{2} R_c$ in the upper 70% of the channel, which implies that $f(Ri)$ is reduced by more than 75% compared to its neutral value. The Ri-profile from the DNS shows a similar shape, tending to a somewhat more neutrally stratified region in the lower half of the channel.

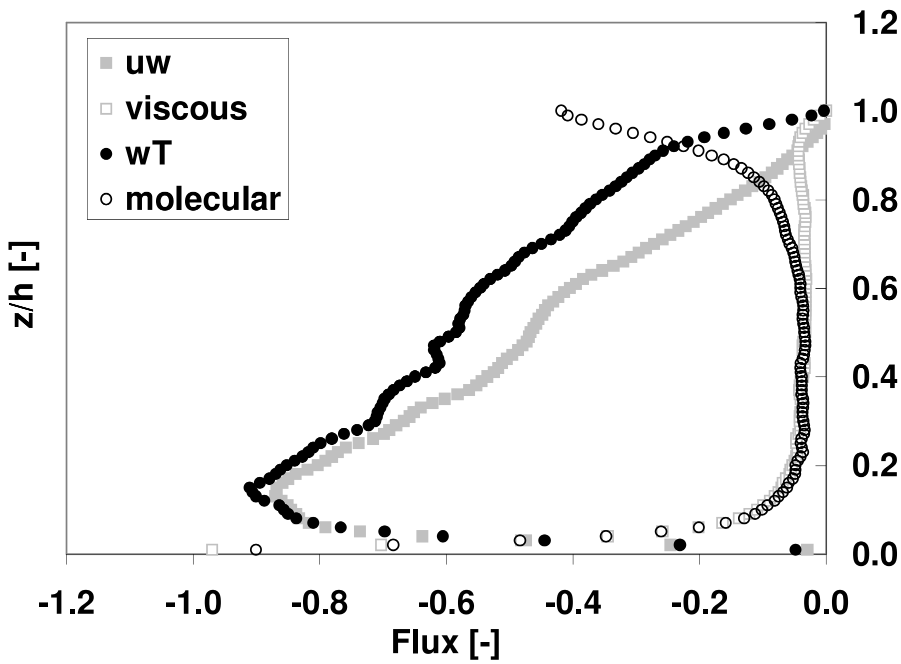

Fig. 7a: instantaneous flux profiles (molecular and turbulent contributions) as calculated by the DNS (slab averages at t=25t*).

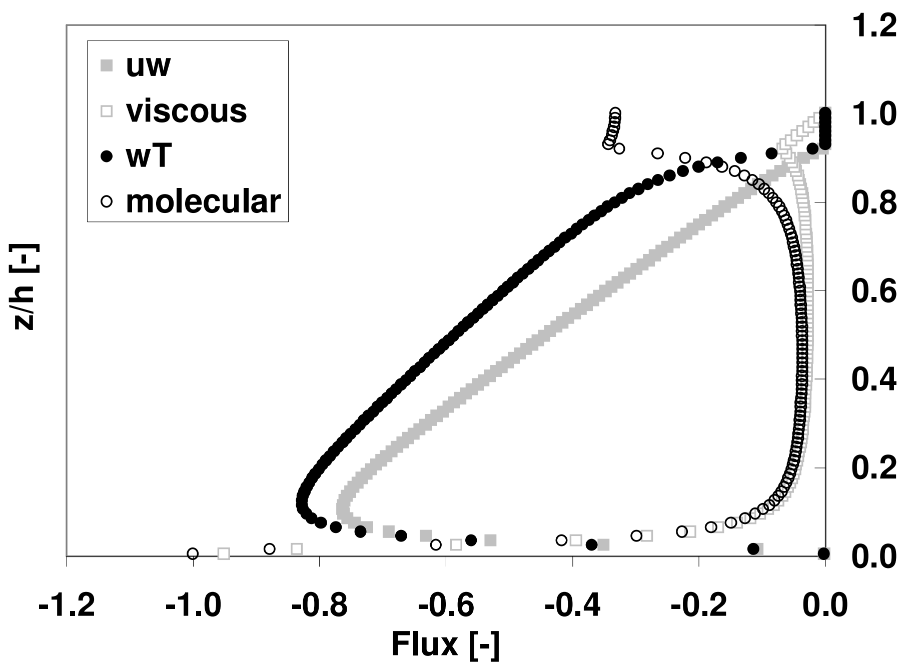

Fig. 7b: as 7a but for the 1-D model.

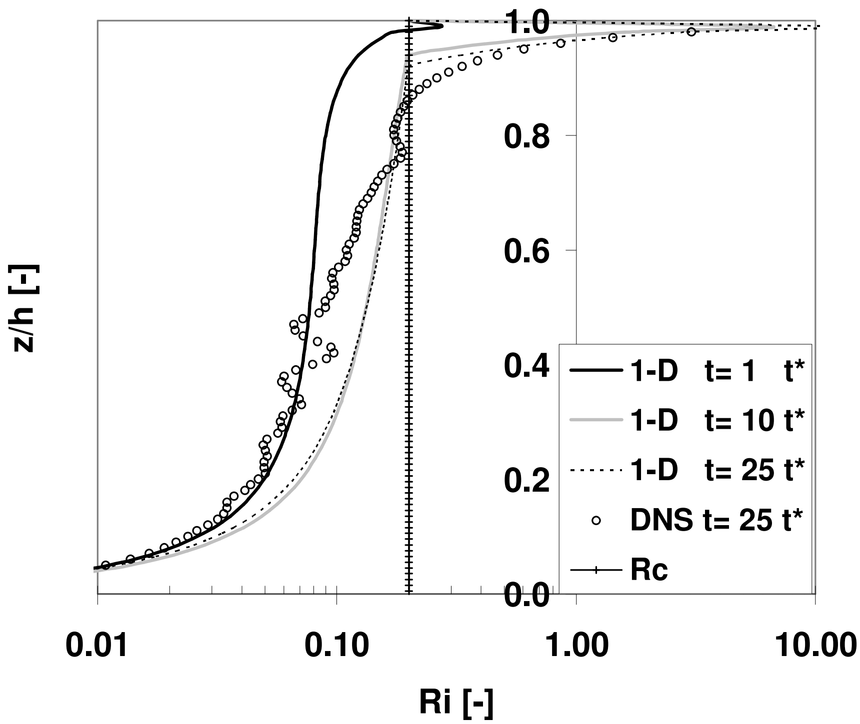

Fig. 8: Time evolution of the Ri-profiles for the 1-D model. For t=25 t* also the DNS profile is depicted. The critical Richardson number (here 0.2) is indicated by the vertical line.

5 Similarity functions from direct numerical simulation

5.1 Flux-profile relationships

From the previous section it appears that the profiles of mean velocity and temperature, as well as the flux-profiles of the DNS are closely approximated by the 1-D model. This result is significant, because the 1-D turbulent closure has its roots in high-*Re* atmospheric flow observations, and is now successfully applied to a low-*Re* turbulent flow. This result suggests that Reynolds similarity holds: results become independent of *Re* when Re is large enough. From this we are encouraged to estimate local similarity functions for mean gradients directly from DNS turbulent fields. Usually the local similarity functions are defined as (Nieuwstadt, 1984):

$$\phi_M \equiv \frac{\partial U}{\partial z}\frac{\kappa z}{u_*} = f(z/\Lambda) \tag{17}$$

$$\phi_H \equiv \frac{\partial \theta}{\partial z}\frac{\kappa z}{\theta_*} = f(z/\Lambda) \tag{18}$$

Local similarity is a generalization of Monin-Obukhov similarity in a sense that local turbulent variables (here: u_*, θ_* or H) are used in stead of surface variables (here: u_{*0}, θ_{*0} or H_0; Sorbjan, 2007). Thus the local Obukhov length Λ is defined as:

$$\Lambda = \frac{\theta_{ref}}{\kappa g} \frac{u_*^2}{\theta_*}$$

(19)

The simulation is run for $t = 102t_*$ in order to reach a quasi-steady state (Fig. 9)

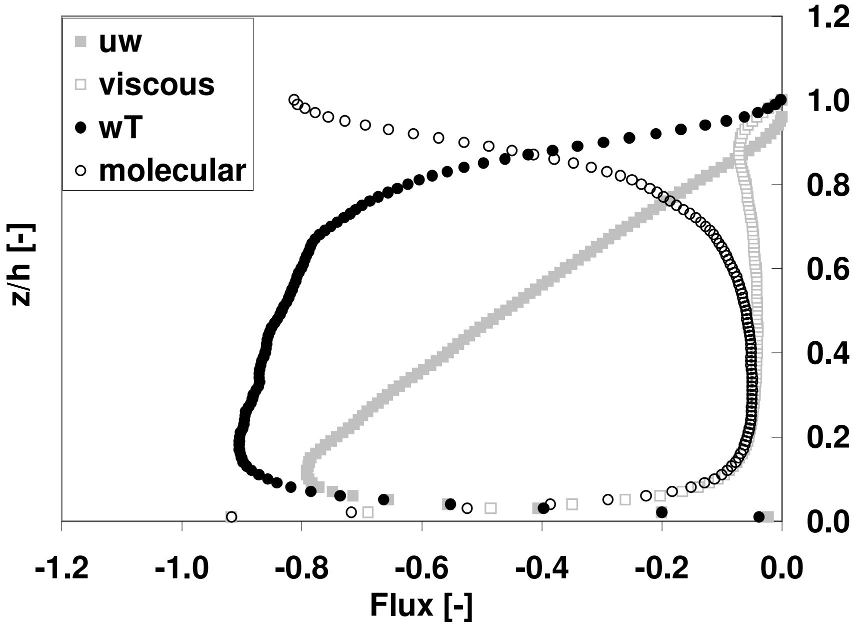

Fig. 9: DNS flux profiles showing quasi-stationary behavior. t=100t*. Averages have been taken over 20 fields between t=100t* and t=102t*.

The turbulent heat flux profile in Fig. 9 becomes almost uniform, suggesting that the system evolves from a quasi-steady towards true-steady state. However, longer integrations with the 1-D model (not shown) reveal that asymptotic steady-state is reached only near $t = O(500t_*)$. For our purpose quasi-steadiness suffices, because a local balance between turbulent fluxes and gradients has settled in.

Next, fluxes and mean variables are spatially and temporally averaged, by taking horizontal slab averages over the period $t = 100t_* - 102t_*$. In this way a statistically robust estimation of the 'ensemble average' is obtained. In the current set-up, vertical gradients of the mean wind and temperature can be estimated directly from finite differences:

a) A large number (100) of computational levels are available, so that finite differences give an accurate estimation of the differentials in (17) and (18) 'in a Taylor-series sense'.
b) Large curvature in the mean variables occurs mainly near the boundaries and those regions are excluded in the analysis (see below).

In the atmosphere, the local similarity functions are hardly influenced by molecular effects, due to the high Reynolds number. Thus, in order to be representative for the atmosphere, the present analysis excludes the boundary regions where molecular effects significantly contribute to the total flux (Fig. 9). As such we exclude the regions: $z/h < 0.15$ and $z/h > 0.75$. After scaling with the local fluxes the dimensionless gradients are obtained as a function of z/Λ (Fig. 10). For comparison also the line $\phi_{M,H} = 1 + 5z/\Lambda$ is plotted.

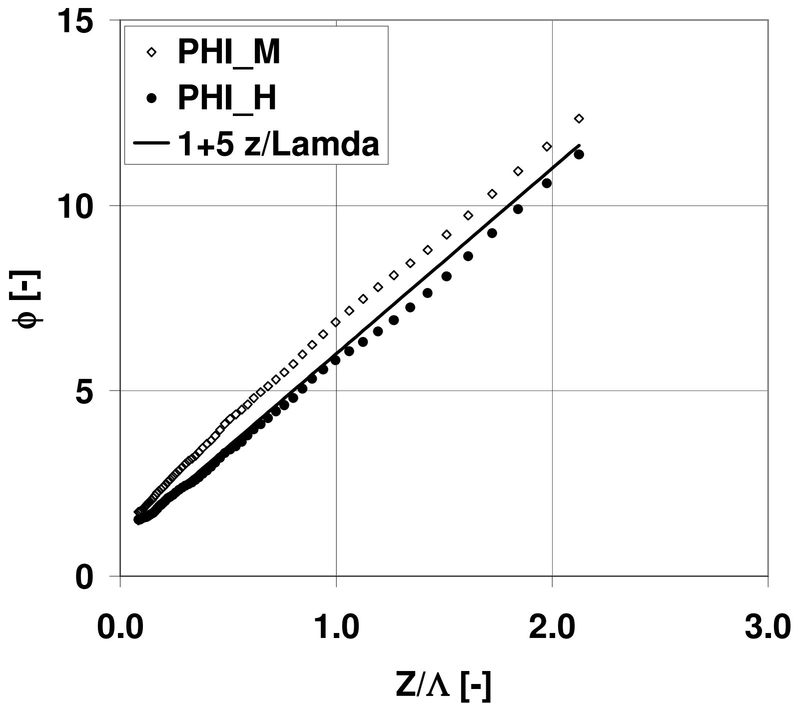

Fig. 10: Dimensionless gradients as a function of the stability parameter z/Λ, as obtained from the DNS. For comparison also the line $\phi_{M,H} = 1 + 5z/\Lambda$ is given.

A clear linear dependence is found over the range of analysis ($0 < z/\Lambda < 2$), i.e. up to moderate stability (in the next section we will show that this linearity also holds for larger ranges of z/Λ). Both curves seem to be reasonably represented by the function $\phi_{M,H} = 1 + 5z/\Lambda$, although it seems that in our case the ϕ_M -graph lies above the ϕ_H -graph. Those marginal differences are likely caused by molecular effects. Although molecular effects are largely excluded from the analysis, their effect may still be noticeable in the mean gradients in the bulk of the boundary layer, since the region dominated by molecular transport acts as the 'boundary condition' for the bulk of the flow. Since in our set-up the upper boundary conditions are essentially different for heat and momentum (compare also Fig. 9), this could be marginally reflected in the Phi-functions.

We note that the ϕ-functions in figure 10 are in general agreement with the classical results of Webb (1970) and Businger et al. (1971). However, those results were obtained for weak stability ($z/\Lambda < O(0.5)$). Ever since, there have been a vast number of experimental studies to extend the ϕ-functions to stronger stability (Beljaars and Holtslag, 1991; Howell and Sun, 1999; Chen and Brutsaert, 2005; Chrachev et al., 2007). For weak stability (say: $z/\Lambda < 1$) most studies show a linear dependence with coefficients typically between 4-8, more or less in agreement with the classical results. For stronger stability however, results rapidly diverge amongst various studies, so that the precise shape of the phi-functions is still under debate. In fact, physically speaking, it is not clear if ϕ_M and ϕ_H *are* still 'universal/unique functions' at large stability. In our opinion, this apparent non-universality in the stability functions may be caused by the fact that observations almost always 'suffer' from non-homogeneity and nonstationarity of the flow. This view is supported by recent findings of Mahrt (2007) from analysis of the FLOSSII dataset. He shows that in stationary conditions ϕ_M generally has a linear shape as in Fig. 10, whereas for non-stationary conditions ϕ_M tends to 'level-off'. For ϕ_H the picture is less clear. In fact similar results where found from our DNS study (not shown) by plotting Fig. 10 for non-stationary situations (i.e. for t:$< 25t_*$), which resulted in leveling-off behaviour for ϕ_M and ϕ_H . Also, we recall that both the flux-calculation (Vickers et al. 2007) and the gradient calculations from a limited number of observational levels (Baas et al., 2006), is far less trivial than in a DNS. Finally, other atmospheric processes, such as long-wave radiative cooling, may directly affect the temperature gradient and distort a unique relationship between gradients and the turbulent fluxes.

5.2 Some sensitivity analysis

As discussed in section 2 the numerical resolution of our simulations (kept equal to N05) is still rather course for a DNS. Therefore, we performed a double resolution run (200^3 grid cells), and repeated the analysis of the previous section. The result is depicted in Fig. 11a. Comparing Fig. 11a with Fig. 10 it appears that the result is resolution-independent and we conclude that the default simulation has sufficient resolution (a comparison of the law-of-the-wall between the two runs showed some grid-dependence, with improved correspondence with the theory for the high resolution run; not shown). With this fact it is tempting to run a higher Reynolds number, e.g. $\mathrm{Re}_* = 720$ .Using 200^3 grid cells this implies that $\Delta z/\eta \cong 1.5$ comparable to the default resolution where $\Delta z/\eta \cong 1.7$ (section 2). Due to the fact that a higher Reynolds number is simulated we need only to exclude a smaller range of z/h in order to reduce molecular effects, i.e. excluding $z/h < 0.08$ and $z/h > 0.85$, so that a larger range of z/Λ is visible in the graph. Comparing Fig. 11b with Fig. 10 reveals that the loglinear character is maintained at the higher Reynolds number. On the other hand a signature of some

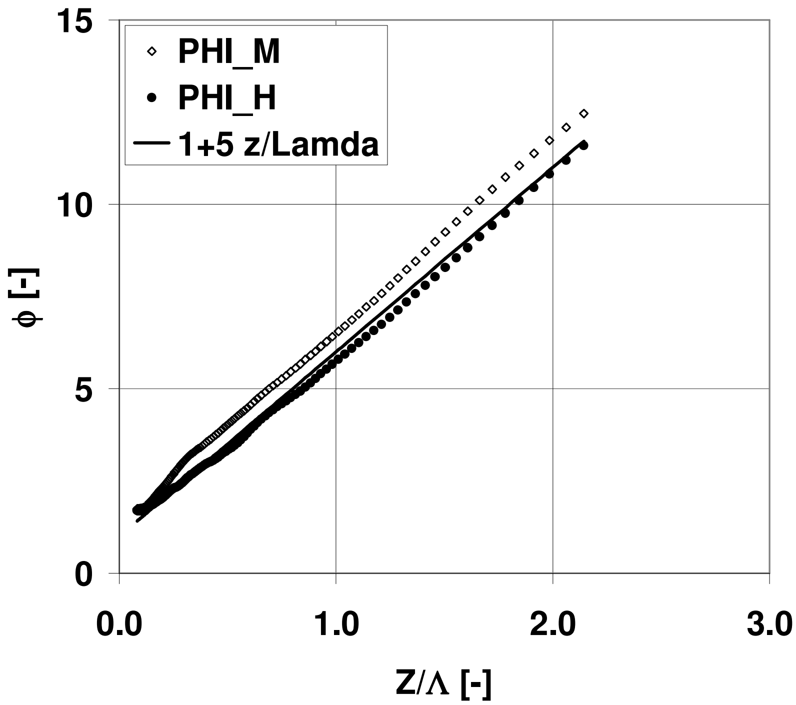

Fig. 11a: as figure 10, thus keeping $\mathrm{Re}_* = 360$, but using double resolution in the simulation.

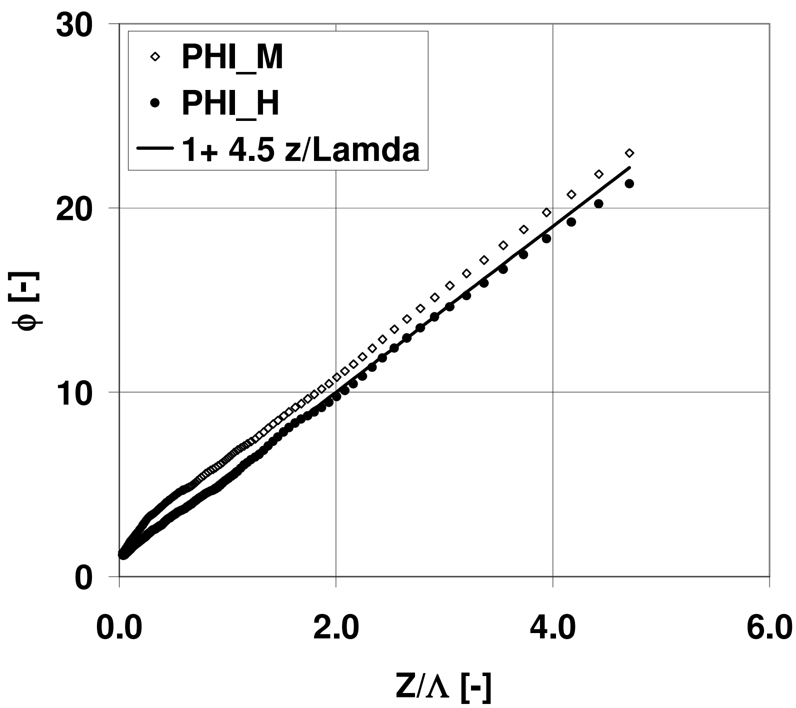

Fig. 11b: as figure 10, but double friction Reynold number: $\mathrm{Re}_* = 720$. Due to higher Reynolds number a larger range of z/Λ outside the viscous range can be plot.

Reynolds dependency of the results is present in the fact that the slope of the graph tends to be closer to 4.5 in stead of 5 in the default case. Although it is beyond the scope of the present work to fully explore Reynolds dependencies of the results, this aspect certainly deserves more attention in future studies.

6 Discussion

6.1 Local scaling

Our DNS results support the idea of local scaling and strongly suggest a log-linear shape of the phi-functions. At this point we recognize that such shape can be anticipated from physical arguments in terms of mixing lengths (Van de Wiel et al. 2008), but can also be inferred from Nieuwstadt's (1984) work. Note that a log-linear shape also implies simple quadratic stability functions in terms of the gradient Richardson number Eq. (12), which facilitates analytical studies on the collapse phenomenon mentioned in the introduction.
On the other hand the present work is far from complete: especially the sensitivity of the results to the Reynolds and Prandtl number could be explored in more depth, and non-stationary or non-homogeneous flows deserve more attention. We also did not address the local scaling behaviour of dimensionless variances or other dimensionless groups (as in Coleman et al. 1992). As such, the main issue of the present work is to support DNS as a useful alternative for Large Eddy Simulations in simulating atmospheric stable boundary layers.

6.2 Implications for the collapse phenomenon

Pioneering studies by McNider (1995), Derbyhire (1999) and Van de Wiel et al. (2002b) revealed that the land-atmosphere feedback is of key-importance for the collapse phenomenon: both top-soil and vegetation must be considered as part of the dynamic system, not as an external boundary condition. As such, flux boundary conditions (as in N05) or temperature boundary conditions are an oversimplification. A realistic study of the collapse phenomenon should include some surface energy balance with a parameterization of the vegetation and include the top-soil where the true temperature boundary condition lies below the e-folding depth where the daily cycle is felt. Realistic boundary conditions are much easier incorporated in single column models than in a DNS. As such, in view of the success of local scaling, 1-D models have potential for studying the collapse phenomenon. On the other hand it is not necessarily obvious that either the 1-D model or the DNS are suitable tools for studying the collapse of turbulence in the SBL:

- Local scaling implies that turbulence should be steady and in local equilibrium. By definition steadiness is absent in decaying turbulence and the similarity model can at best only serve as a crude approximation for this type of flow (when $\partial TKE/\partial t$ is relatively small compared to the other terms in the turbulent kinetic energy equations).
- On the other hand, the SBL simulations by DNS, though valid in itself, may loose their analogy to *atmospheric* SBL's: in ceasing turbulence the effective Reynolds number will significantly decrease and simulated results will be dominated more and more by viscous effects. In the atmosphere however, viscosity dominated flow will not easily occur, even when turbulence is very weak (Mahrt and Vickers, 2006).

Therefore, in future work we will investigate the collapse phenomenon by using both models in order to find an answer to those issues.

7 Conclusions

In the present work a continuous turbulent stably stratified channel flow is studied with a direct numerical simulation model and with a simple similarity model. With DNS, the flow is simulated without the need of a specific turbulence closure model, whereas the local similarity model is based on a simple parameterization of turbulence. A relatively low Reynolds flow (O (7000)) is simulated and both models explicitly account for molecular flux contributions. The flow configuration is identical to the flow configuration by Nieuwstadt (2005), who studied both the continuous turbulent and the collapsed SBL. The present work only addresses the continuous turbulent part with the following conclusions:

- The evolution of the profiles of mean and the flux profiles show a remarkably close agreement between the 1-D model and the DNS. This is surprising because the 1-D model originates from high Reynolds number similarity laws and is successfully applied to low Re, so that the dependence on the exact Reynolds number seems to be weak.
- From this fact, (low-Re) Direct Numerical Simulations have potential as a tool (complementary to atmospheric observations) to find similarity relationships such as local scaling relations. With the DNS pure stationary and homogeneous flow can be simulated, whereas those conditions are rarely encountered in reality. The dimensionless gradients of wind and temperature from our DNS show strong evidence for log-linear behaviour close to the traditional $\phi_{M,H} = 1 + 5z/\Lambda$, over the range of analysis ($0 < z/\Lambda < 4$). On the other hand, the current analysis is based on low *Re* flow and the sensitivity of the results on *Re* deserves more attention in future work.

Literature

Baas P., G. J. Steeneveld, B. J. H. Van de Wiel, A. A. M. Holtslag, 2006: Exploring Self-correlation in flux-gradient relationships for stably stratified conditions. *J. Atmos. Sci.,* **63**, 3045-3054.

Banta, R. M., L. Mahrt, D. Vickers, J. Sun, B. B. Balsley, Y. L. Pichugina, and E. J. Williams, 2007: The very stable boundary layer on nights with weak low level jets., *J. Atmos. Sci.* **64**, 3068-3090.

Basu, S., F. Porté-Agel, E. Foufoula-Georgiou, J-F. Vinuesa, M. Pahlow, 2006: Revisiting the local scaling hypothesis in stably stratified atmospheric boundary layer turbulence: an integration of field and laboratory measurements with large-eddy simulations. *Bound-Layer Meteorol*, **119**, 473-500.

Beljaars, A. C. M., and A. A. M. Holtslag, 1991: Flux parametrization and land surfaces in atmospheric models. *J. Applied Meteor.* **30**, 327-341.

Beljaars, A. C. M., and P. Viterbo, 1998: Role of the boundary layer in a numerical weather prediction model. *Clear and Cloudy Boundary Layers*, Holtslag A. A. M., P. G. Duynkerke, and P. J. Jonker Eds., Royal Netherlands Ac. Of Arts and Sci., Amsterdam, 287-304.

Businger, J. A., J. C. Wyngaard, Y. Izumi, and E. F. Bradley, 1971: Flux-profile relationships in the atmospheric boundary layer. *J. Atmos. Sci.,* **30**, 788-794.

Cheng, Y., and W. Brutseart, 2005: Flux-profile relationships for wind speed and temperature in the stable atmospheric boundary layer, *Bound-Layer Meteorol*, **114**, 519-538.

Coleman, G. N., J. H. Ferziger, P. R. Spalart, 1992: Direct simulation of the stably stratified turbulent Ekman layer, *J. Fluid Mech*., **244**, 677-712.

Derbyshire, S. H., 1999a: Stable boundary layer modelling: established approaches and beyond. *Bound. Layer Meteor.,* **90**, 423-446.

Derbyshire, S. H., 1999b: Boundary-layer decoupling over cold surfaces as a physical boundary instability. *Bound. Layer Meteor.*, **90**, 297-325.

Galmarini, S., C. Beets, P. G. Duynkerke, and J. Vila-Guerau de Arellano, 1998: Stable nocturnal boundary-layers: a comparison of one-dimensional and large-eddy simulation models. *Bound. Layer Meteor.*, **88**, 181-210.

Grachev, A. A., E. L. Andreas, C. W. Fairall, P. S. Guest, and P. O. G. Persson, 2007: SHEBA flux-profile relationships in the stable atmospheric boundary layer. *Bound. Layer Meteor.*, **124**, 315-333.

Högström, U., 1996: Review of some basic characteristics of the atmospheric surface layer. *Bound. Layer Meteor.*, **78**, 215-246.

Howard, L. N., 1961: Note on a paper of John W. Miles. *J. Fluid Mech.*, **13**, 158-160.

Howell, J. F., and J. Sun, 1999: Surface-layer fluxes in stable conditions. *Bound. Layer Meteor.*, **90**, 495-520.

Kundu, P. K., 1990: *Fluid Mechanics.,* Academic Press, San Diego.

Malhi, Y. S., 1995: The significance of the dual solutions for heat fluxes measured by the temperature fluctuation method in stable conditions. *Bound. Layer Meteor.*, **74**, 389-396.

Mahrt L., J. Sun, W. Blumen, T. Delany, and S. Oncley, 1998: Nocturnal boundary layer regimes. *Bound. Layer Meteor.*, **88**, 255-278.

Mahrt L., 1998: Statified atmospheric boundary layers and breakdown of models, *Theoret. Comput. Fluid Dynamics*, **11**: 263-279.

Mahrt L., 1999: Stratified atmospheric boundary layers. *Bound. Layer Meteor.*, **90**, 375-396.

Mahrt L., D. Vickers, R. Nakamura, M. R. Soler, J. Sun, S. Burns, D. H. Lenschow, 2001: Shallow drainage flows. *Bound. Layer Meteor.*, **101**, 243-260.

Mahrt, L., and D. Vickers, 2006: Extremely weak mixing in stable conditions. *Bound. Layer Meteor.*, **119**, 19-39.

Mahrt, L., 2007: The influence of nonstationarity on the turbulent flux-profile relationships for stable stratification. *Bound. Layer Meteor.*, **125**, 245-264.

McNider, R. T., D. E. England, M. J. Friedman, and Shi, X., 1995: Predictability of the stable atmospheric boundary layer. *J. Atmos. Sci.* **52**, 1602-1614.

Miles, J. W., 1961: On the stability of heterogeneous shear flows. *J. Fluid Mech.*, **10**, 496-508.

Nappo, C. J., and P-E Johansson, 1999: Summary of the Lövånger international workshop on turbulence and diffusion in the stable planetary boundary layer. *Bound. Layer Meteor.*, **90**, 345-374.

Newsom, R. K., and R. M. Banta, 2002: Shear-flow instability in the stable nocturnal boundary layer as observed by Doppler lidar during CASES99., *J. Atmos. Sci.* **60**, 16-33.

Nieuwstadt, F. T. M., 1984: The turbulent structure of the stable, nocturnal boundary layer. *J. Atmos. Sci.* **41**, 2202-2216.

Nieuwstadt, F. T. M., 1992: *Turbulentie: inleiding in the theorie en toepassingen van turbulente stromingen*. Epsilon Uitgaven, Utrecht, 202 pp.

Nieuwstadt, F. T. M., 2005: Direct numerical simulation of stable channel flow at large stability. *Bound. Layer Meteor.,* **116**, 277-299.

Pope, S. B., 2000: *Turbulent Flows*, Cambridge University Press, U.K.

Poulos, G. S., W. Blumen, D. Fritts, J. L. Lundquist, J. Sun, S. P. Burns, C. Nappo, R. Banta, R. Newsom, J. Cuxart, E. Terradellas, B. Balsey, and M. Jensen, 2002: CASES-99: A comprehensive investigation of the stable nocturnal boundary layer. *Bull, Amer. Meteor. Soc*., **83**, 555-581.

Sorbjan, Z., 2006: Local structure of turbulence in stably stratified boundary layers. *J. Atmos. Sci*., **63**, 1526-1536.

Sun, J., D. H. Lenschow, S. P. Burns, R. M. Banta, R. K. Newsom, R. Coulter, S. Frasier, T. Ince, C. Nappo, B. B. Balsey, M. Jensen, L. Mahrt, D. Millar, and B. Skelly, 2003: Atmospheric disturbances that generate intermittent turbulence in nocturnal boundary layer. *Bound. Layer Meteor.*, **110**, 255-279.

Sun, J., S.P. Burns, A. C. Delany, S. P. Oncley, T. W. Horst, and D. H. Lenschow, 2003: Heat balance in the nocturnal boundary layer during CASES-99. *J. Applied Meteor.,* **42**, 1649-1666.

Steeneveld, G.J., van de Wiel, B.J.H., Holtslag, A.A.M., 2006: Modeling the evolution of the atmospheric boundary layer coupled to the land surface for three contrasting nights in CASES-99, *J. Atmos. Sci.,* **63**, 920-935.

Van de Wiel, B. J. H., R. J. Ronda, A. F. Moene, H. A. R. De Bruin, and A. A. M. Holtslag, 2002a: Intermittent turbulence and oscillations in the stable boundary layer. Part I: A bulk model. *J. Atmos. Sci*., **59**, 942-958.

Van de Wiel, B. J. H., A. F. Moene, R. J. Ronda, H. A. R. De Bruin, and A. A. M. Holtslag, 2002b: Intermittent turbulence and oscillations in the stable boundary layer. Part II: A system dynamics approach. *J. Atmos. Sci.,* **59**, 2567-2581.

Van de Wiel, B. J. H., A. F. Moene, O. K. Hartogensis, H. A. R. De Bruin, and A. A. M. Holtslag, 2002: Intermittent turbulence and oscillations in the stable boundary layer. Part III: A Classification for observations during CASES99. *J. Atmos. Sci.,* **60**, 2509-2522.

Van de Wiel, B. J. H. , Moene A. F., Steeneveld G. J., Hartogensis O. K., Holtslag A. A. M., 2007: Predicting the Collapse of Turbulence in Stably Stratified Boundary Layers. *Flow Turbulence and Combust.*, **79**, 251-274.

Van Driest, E. R. , 1956: On turbulent flow near a wall. *J. Aerospace Sci.,* **23**, 1007-1011.

Vickers D., and L. Mahrt, 2006: A solution for flux contamination by mesoscale motions with very weak turbulence. *Bound. Layer Meteor.*, **118**, 431-447.

Webb, E. K., 1970: Profile relationships: The log-linear range, and extension to strong stability, *Quart. J.R. Met. Soc.*, **96**, 67-90.